Int. J. Heat Mass Transfer. Vol. 35, No. 8, pp. 1957–1968, 1992
Printed in Great Britain

0017–9310/92 $5.00 + 0.00

Turbulent gas flux measurements below the air–water interface of a grid-stirred tank

CHIA REN CHU and GERHARD H. JIRKA
DeFrees Hydraulics Laboratory, Cornell University, Ithaca, NY 14853, U.S.A.

(*Received* 13 *February* 1991 *and in final form* 6 *August* 1991)

Abstract—Experiments have been conducted in an effort to elucidate the details of the interfacial gas transfer mechanism under liquid-side control. Near-surface liquid turbulence and oxygen concentration fluctuations have been measured in a laboratory grid-stirred tank for a range of turbulent Reynolds number R_L from 80 to 660. Our observations show that the thickness of the gas boundary layer closely agrees in trend and magnitude with the Lewis–Whitman's film thickness as determined from the bulk concentration change. Furthermore, the functional dependence on turbulent Reynolds number is consistent with a large eddy domination. Additional simultaneous measurements of turbulent velocity and oxygen concentration fluctuations, including direct flux measurements, give further indication that the large scale eddy motions are more effective in the interfacial mass transfer process.

INTRODUCTION

THE TRANSFER processes across the gas/liquid interface are of fundamental importance to the understanding of the distribution of many substances in the natural environment and to the control of engineering processes. In most cases, it is desired to predict the transfer rate of a particular substance across the interface. The transfer rate is usually determined by the properties of the substance and also the hydrodynamic condition of both phases. For low solubility gases, such as oxygen, it is well established that the resistance on the liquid side controls the transfer process (Coantic [1]).

Customarily, the gas transfer rate is parameterized by the liquid phase gas transfer coefficient (or transfer velocity) K_L

$$J = -K_L(C_s - C_b) \tag{1}$$

where J is the gas flux per unit interfacial area, and C_s and C_b are the saturated and bulk concentration of dissolved gas, respectively.

Although numerous theoretical models and empirical formulations have been proposed over the years, there is still no general agreement on the calculation of the gas transfer rate. This is because the relation between liquid turbulence and interfacial mass transfer still remains unresolved. Despite an abundance of conceptual models and paradigms which picture the gas transfer process with distinct flow structural and/or statistical properties (for a summary of those models see Coantic [1], Theofanous [2], Brumley and Jirka [3]), there is a paucity of direct measurements that provide inspection into the actual mechanism. Clearly, the difficulty for direct measurements lies in the small dimensions of the gas boundary layer, especially under high turbulence conditions, and its time-varying location (waviness).

Recent attempts for direct measurements of the transfer mechanism within the gas boundary layer have been reported by Luk and Lee [4], Asher and Pankow [5], Jirka and Ho [6], Jähne [7], and Wolff *et al.* [8]. However, none of these experiments has simultaneously measured turbulent velocity and gas concentration in the near-surface region. Such combined measurements are needed to provide further insight into the mechanics of the overall transfer process which is dominated by the interplay of turbulent advection and molecular diffusion, and to, ultimately, validate any of the existing conceptual models.

Estimations of the thickness of the interfacial region in which measurements have to be performed can be made as follows.

The thickness of the gas boundary layer δ can be related to the transfer velocity by a Lewis–Whitman [9] film calculation

$$\delta = D/K_L \tag{2}$$

where D is the molecular diffusivity of the gas. Alternatively, Brumley and Jirka [3] used hydrodynamic arguments to estimate the thickness of an outer diffusive layer L_D below the surface

$$L_D \propto L R_L^{-1/2} Sc^{-1/2} \tag{3}$$

where L is the integral length scale of liquid turbulence, $R_L = uL/\nu$ is the turbulent Reynolds number, with u the velocity scale of turbulence, ν the kinematic viscosity of water, and Sc the Schmidt number of the gas. From either equation (2) or (3), the thickness of the interfacial region is of the order of 100 μm for typical environmental turbulence conditions. This means that the dimension of a measuring sensor has to be smaller than 10 μm in order to provide sufficient resolution inside the interfacial region.

Grid-stirred tanks have been used by many

NOMENCLATURE

C	oxygen concentration
C_b	oxygen concentration at the bulk region
C_s	saturated oxygen concentration
C_{wc}	coincident spectral density function
c	fluctuation component of concentration
c'	r.m.s. of concentration fluctuation
D	molecular diffusivity of dissolved oxygen
E_{wc}	cross-spectrum of velocity and concentration
f	oscillation frequency of grid
H	water depth
J	gas flux across the interface
K_L	gas transfer coefficient, or transfer velocity
L	integral length scale of turbulence
L_B	Batchelor sublayer
L_c	integral length scale of concentration
L_D	diffusive sublayer
L_V	viscous sublayer
L_w	integral length scale of vertical velocity
L_∞	longitudinal integral length scale far from the surface
M	mesh size of grid
Q_{wc}	quadrature spectral density function
R_L	turbulent Reynolds number
R_{wc}	cross-correlation function of velocity and concentration
S	grid stroke
Sc	Schmidt number
u	characteristic turbulent velocity
U_{HT}	Hopfinger–Toly velocity
W	vertical velocity
w	fluctuation component of vertical velocity
w'	r.m.s. of vertical velocity fluctuation
y	distance from the virtual origin
Z_s	distance from virtual origin to the water surface
z	vertical coordinate upward from water surface
z_0	measured gas boundary layer thickness.

Greek symbols

α	scaling constant for z_0
β	scaling constant for K_L
δ	Lewis–Whitman film thickness
η	Kolmogorov sublayer
κ_1	one-dimensional wave number
ν	kinematic viscosity of water.

researchers for interfacial transfer study because of their reproducible and well controlled turbulent environment. In a grid-stirred tank, turbulent eddies are generated at some distance below the surface and decay as they diffuse toward the surface. Although the way of generating turbulence is different from that of an open channel flow, the interaction between the turbulence and surface has many common features.

Hopfinger and Toly [10] have shown that a vertically oscillating grid can be used to produce horizontally near-homogeneous turbulence, and the r.m.s. horizontal velocity u' in a grid-stirred tank can be related to easily measured parameters such as grid stroke S, oscillation frequency f, and mesh size M

$$u' = 0.25 f S^{1.5} M^{0.5} y^{-1} \tag{4}$$

where y is the distance from a virtual origin approximately at the center of the grid stroke.

In finite tank depth conditions with a free surface, Brumley and Jirka [11] found the spatially averaged velocity fluctuations in the bulk region of a grid-stirred tank agreed well with equation (4). However, the turbulent structure is affected by the presence of the surface with a 'surface-influenced layer', whose thickness is

$$L_\infty = 0.1 Z_s \tag{5}$$

where L_∞ is the longitudinal integral length scale far from the surface, Z_s is the distance from the surface to the virtual origin. This can be explained by the irrotational source theory of Hunt and Graham [12]. This theory assumes that the effect of a shear-free surface on a homogeneous turbulence field is the instantaneous superposition of an irrotational velocity field which cancels out the vertical velocity fluctuations. Brumley and Jirka [11] used the velocity at the surface ($y = Z_s$), computed from equation (4), as a velocity scale to characterize the different turbulence conditions, and called this velocity the Hopfinger–Toly velocity U_{HT}

$$U_{HT} = 0.25 f S^{1.5} M^{0.5} Z_s^{-1}. \tag{6}$$

The present paper describes measurements of turbulent velocity and fluctuating gas (oxygen) concentration by means of a split hot-film and an oxygen microprobe, respectively, near the air–water interface in a grid-stirred tank. The objective is to elucidate the details of the surface transfer mechanisms, including the structure of up- and down-welling motions and the existence and extent of various hydrodynamic and diffusive boundary layers.

EXPERIMENTAL APPARATUS

The experiments were carried out in a 40 cm-deep, 50 cm-square tank with a vertically oscillating grid. Turbulence measurements were conducted by means of a rotating split-film anemometer (1.3 mm sensing-length quartz coated platinum films at the top and bottom of a 0.153 mm diameter cylindrical fiber)

which allowed measurements of the horizontal and vertical velocity fluctuations. A full description of the grid-stirred tank and split-film anemometer is given by Brumley and Jirka [11].

The polarographic oxygen microprobe was built by modifying the procedure described by Lee *et al.* [13]. A piece of pure platinum wire (50 μm diameter and 15–20 mm long) was fused to a length of 0.5 mm diameter copper wire using silver solder paint. The tip portion of the platinum wire was electrolytically etched in a sodium nitrite ($NaCO_2$) solution to 1.0–2.0 μm. A pipette puller was then used to collapse a glass capillary tubing (1.1 mm o.d., 50 mm long) onto the etched platinum wire. A microelectrode with tip diameter less than 5 μm is quite reproducible with this technique.

The finished microprobe was coated with a polystyrene solution in order to provide a gas-permeable membrane for the electrode. The copper wire left outside of the glass tubing was soldered to a wire wrap wire and insulated with a piece of thermal shrinking tubing. The entire probe was then mounted on a stainless steel tubing. The other end of the wire wrap wire sticking out of the steel tubing was soldered to a BNC connector. A special aluminum connector holder was built to fix the BNC connector with the steel tubing. Figure 1 shows a picture of the finished oxygen microprobe. Further details of probe construction are given by Chu [14].

The principle of polarographic electrodes consists of applying a negative voltage on a cathode with respect to an anode in an electrolyte solution. The dissolved gas reduced at the surface of the cathode will cause an electrical current to flow. The current output of the electrode is directly proportional to the partial pressure of gas, which in turn can be related to the concentration of dissolved gas.

The output current from the microprobe was amplified by a picoammeter (range 10^{-8}–10^{-12} A). The microprobes were calibrated against the readings of a commercial oxygen sensor (Beckman Monitor II Oxygen Analyzer). The probe response time was determined by passage of the rotating microprobe through a laminar double jet flow. This jet flow was produced by separating a round jet orifice (1 cm diameter) into two halves by insertion of a razor blade divider and by supplying two water inflows with oxygen concentrations different from each other and from the bulk concentration. The signal output when passing the probe in front of the orifice—so that the interfaces (mixing layers) within the jet and at the jet boundary are very thin—is shown in Fig. 2. A probe time constant (63% response) of about 10 ms can be deduced from Fig. 2. Probes showing a response time of less than 20 ms were employed in this study.

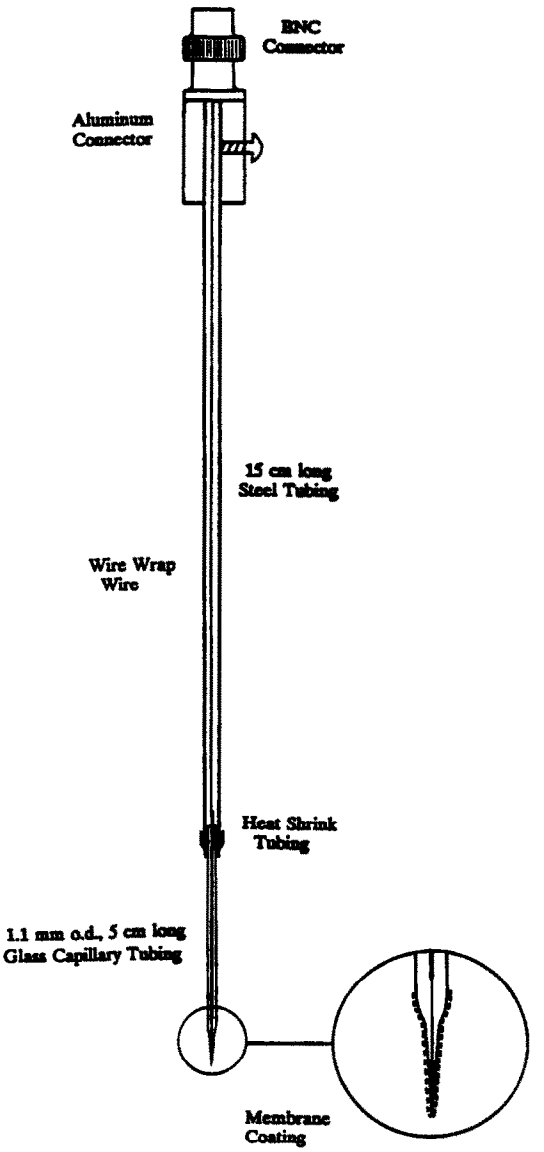

FIG. 1. A finished oxygen microprobe.

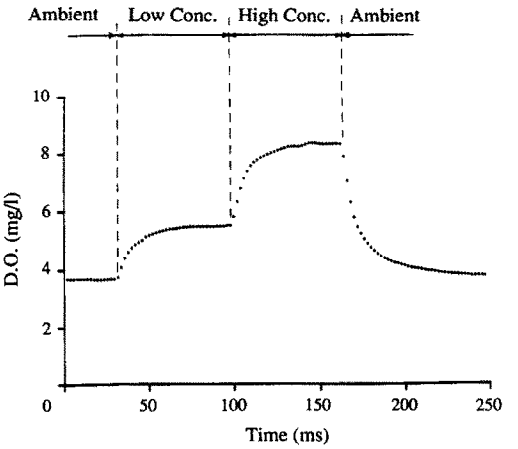

FIG. 2. Step response curve of an oxygen microprobe.

EXPERIMENTAL PROCEDURE

This study is mainly concerned with the specific case of oxygen transfer across a shear-free surface.

Table 1. Experimental conditions

Grid condition set	Grid frequency f (Hz)	Stroke S (mm)	Z_s (mm)	U_{HT} (mm s^{-1})	R_L	C_s (mg l^{-1})	$K_L \times 10^{-4}$ (cm s^{-1})
1	1.63	101	245	13.30	660	9.01	8.89
2	2.56	50	246	7.27	360	8.23	7.90
3	1.28	50	248	3.64	180	8.30	5.23
4	1.66	24	248	1.57	80	8.33	2.61

Two types of experiments were carried out in this study. The first type, called the 'interfacial concentration measurement', used the oxygen microprobe to measure the oxygen concentration in the interfacial region. The second type, called the 'simultaneous measurements', used the split-film probe and the microprobe to measure velocity and concentration fluctuations at the same time. Each type of measurement was carried out for four different turbulence conditions listed in Table 1.

The turbulent Reynolds number is defined as $R_L = 2U_{HT}L_\infty/\nu$, with $u = U_{HT}$, $L = 2L_\infty$. The factor 2 arises because the longitudinal integral length scale L_∞ is theoretically half as large as the length scale for isotropic turbulence (Tennekes and Lumley [15]). The transfer velocities of each turbulence condition are measured by using an oxygen meter to monitor the bulk concentration and temperature changes over 10 h.

Table 2 gives the corresponding thickness of various hydrodynamic and diffusive layers, which can be estimated by the scaling arguments of Brumley and Jirka [3], for the turbulence conditions studied in this paper. The Schmidt number is taken as $Sc = 488$, at 20°C, 1 atm.

In the actual experiment the tank was filled with distilled water to the desired depth. The water was then deoxygenated by bubbling nitrogen into the water for about 15 min. The initial concentration of dissolved oxygen was found to be around 3.5 mg l^{-1} on average. The water surface was skimmed by a specially designed skimmer to reduce surface contamination. The water surface was reasonably clean after the skimming. However, compared with Asher and Pankow's [5] rayon/vacuum cleaned surface, the surface was not as clean.

The tips of the probes were then adjusted to the water surface to set the reference position with zero submergence. In order to let the turbulence in the tank reach a steady state condition, the grid motor was turned on at least 10 min before the first measurements were taken. The probes were then adjusted to the desired submergence with the help of a linear slide (Velmex) on the rotating arm. The linear slide can allow precise vertical positioning to 10 μm spatial resolution.

The probes were rotated in a horizontal circle of 0.76 m circumference with a constant speed of 60 mm s^{-1} during the measurements. At each submergence, 10400-point (4-turn) data from the anemometer and/or the picoammeter were read into the computer. The sampling frequency was 200 Hz for each channel so that scales beyond the Kolmogorov scale could be resolved. The data were then analyzed on a MicroVax II computer.

In the interfacial concentration measurement, both moving probe and stationary probe methods were employed. For the moving probe experiment, the microprobe was travelling along a horizontal circle, which is the same path as in the simultaneous measurement. In the stationary probe experiment, the oxygen microprobe was fixed at one position, namely, 12.3 cm from center, 25.0 cm from both sides of the wall. This corresponds to one point in the circular path of the moving probe measurement. The vertical profile of mean values and r.m.s. concentration from fixed and moving probe measurements, respectively, for grid condition #3, are given in Figs. 3 and 4, and show, by

Table 2. Thickness of various hydrodynamic and diffusive layers†

Grid condition set	Surface influenced layer L_∞ (mm)	Viscous sublayer L_V (mm)	Kolmogorov sublayer η (mm)	Diffusive sublayer L_D (mm)	Batchelor sublayer L_B (mm)
1	24.5	0.97	0.38	0.09	0.017
2	24.6	1.32	0.60	0.12	0.027
3	24.8	1.86	1.02	0.17	0.046
4	24.8	2.80	1.87	0.25	0.085

† The viscous sublayer $L_V = L_\infty R_L^{-1/2}$ is the scale for viscous effects near the free surface. The Kolmogorov sublayer $\eta = 2L_\infty R_L^{-3/4}$ is the length scale of the smallest eddies. The outer diffusive sublayer $L_D = 2L_\infty R_L^{-1/2} Sc^{-1/2}$ can be thought of as the diffusive length scale arising from the largest eddies. The Batchelor sublayer $L_B = \eta Sc^{-1/2}$ represents the diffusive scale caused by the smallest eddies.

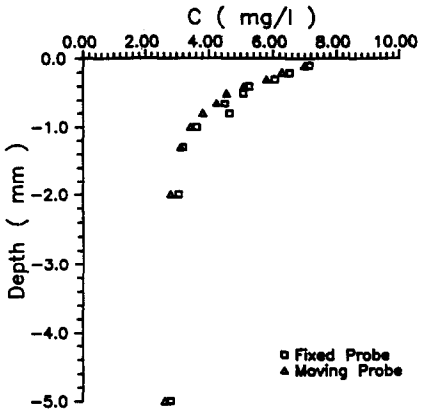

FIG. 3. Mean concentration profile of grid condition #3.

and large, good qualitative and quantitative agreement. This indicates that the fluctuating concentration field is horizontally homogeneous within the interfacial region.

For the simultaneous measurements, the split-film probe and the oxygen microprobe were both positioned on the rotating arm together, in close vicinity to each other. The tip of the oxygen microprobe was kept at the same level as the nominal plane of the split of the split-film probe. The distance between these two probes was about 1.0 mm with the oxygen probe first in the direction of travel (see Fig. 5).

The bulk transfer measurements were done by a commercial oxygen probe (Beckman Monitor II). It was found that the output of this D.O. meter was flow sensitive. In order to meet the 10 cm s^{-1} minimum flow rate requirement close to the probe, the measurements were taken in a pump-through flow cell which was attached externally to the tank.

Surface ripples were observed during the experiments. It was found that the frequency of surface waves was approximately equal to the grid frequency, and the wave heights (peak to trough) were in a range from 0.08 to 0.5 mm, depending on the grid conditions. The vertical irrotational velocity caused by these surface waves can be a substantial fraction of the turbulent intensity in the near-surface region, but will gradually decay as the submergence increases.

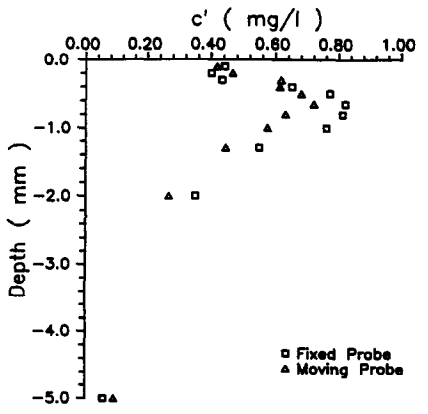

FIG. 4. R.m.s. concentration profile of grid condition #3.

RESULTS AND DISCUSSION

Gas concentration fluctuations

Time series data of gas concentrations for grid condition #3 at 0.1, 0.4, 0.8 and 5.0 mm submergence are shown in Fig. 6. Note that these measurements are juxtaposed for illustration purposes only, and do not represent simultaneous conditions. The concentrations have been normalized as $(C-C_b)/(C_s-C_b)$. The saturation concentration C_s was determined by the method discussed in Ho [16], and shown in Table 1. As can be seen, the concentration at different depths fluctuates at different levels of saturation. The mean concentration at 0.1 mm is reasonably close to the saturation value, and the fluctuations are limited by the saturation value. At 5.0 mm depth, besides occasional small spikes, the concentrations are almost equal to the bulk concentration.

Figure 7 shows the normalized gas concentration profile from the exploratory work of Jirka and Ho [6] compared with the present measurements for the same turbulence condition (grid condition #2). The measurements are in good agreement.

The mean concentration profiles of four different grid conditions are shown in Fig. 8. The profiles for high turbulence conditions have a steeper gradient than those for low turbulence conditions. This indicates that higher turbulence conditions clearly limit the thickness of the mean gas boundary layer. In order to provide simple estimates of the spatial extent of the mean gas boundary layer, exponential curves (solid lines in Fig. 8) of the type

$$\frac{C-C_b}{C_s-C_b} = \exp\left(\frac{z}{z_0}\right) \tag{7}$$

were best-fitted to each grid condition, where z is the vertical coordinate upward from water surface. The regression constant z_0 (with length dimension) can be interpreted as a measured gas boundary layer thickness.

The normalized concentration measurements in which the submergence z has been scaled by z_0 are summarized in Fig. 9(a) for the mean, and Fig. 9(b) for the r.m.s. fluctuation, $c'/(C_s-C_b)$. All these profiles fall together indicating that z_0 is an appropriate length scale for the concentration boundary layer. Surprisingly, the maximum values of r.m.s. concentration occur fairly deep, namely, around $(1–3)z_0$ below the water surface. This suggests that downwelling motions cause significant fluctuations at distances well below the mean boundary layer thickness. This view is consistent with the flow visualization work of Asher and Pankow [5] and the interpretations of Hunt [17].

A display of the directly measured boundary layer thickness z_0, the computed Lewis–Whitman film

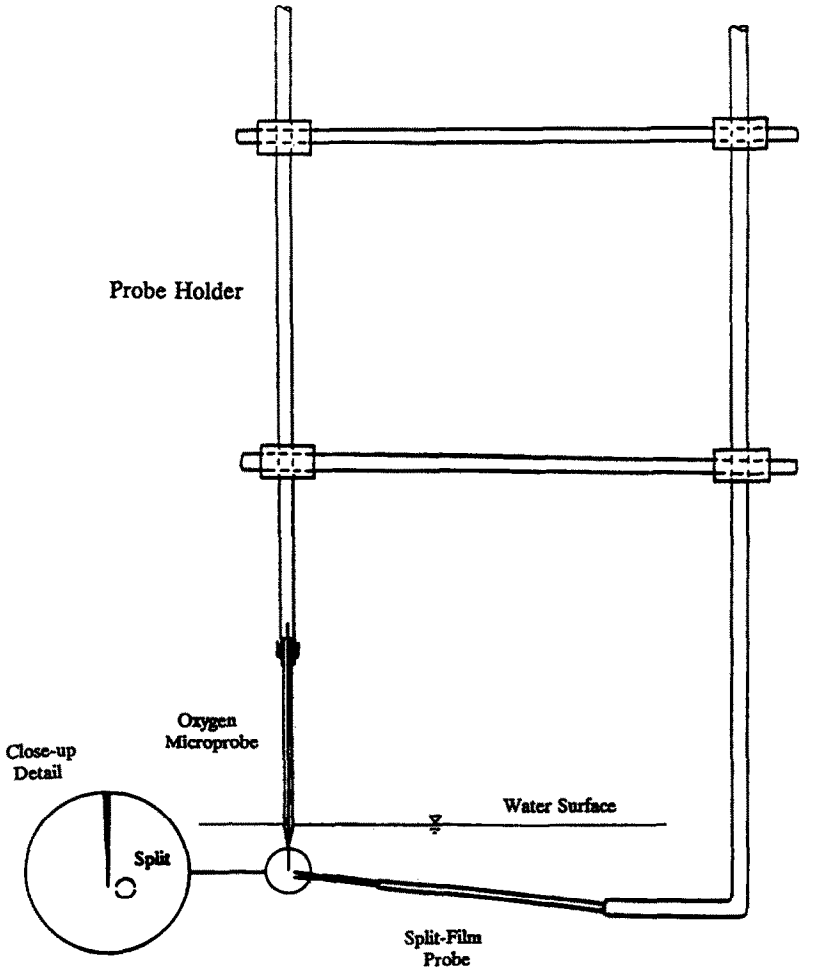

FIG. 5. A sketch of the relative position of split-film probe and oxygen microprobe.

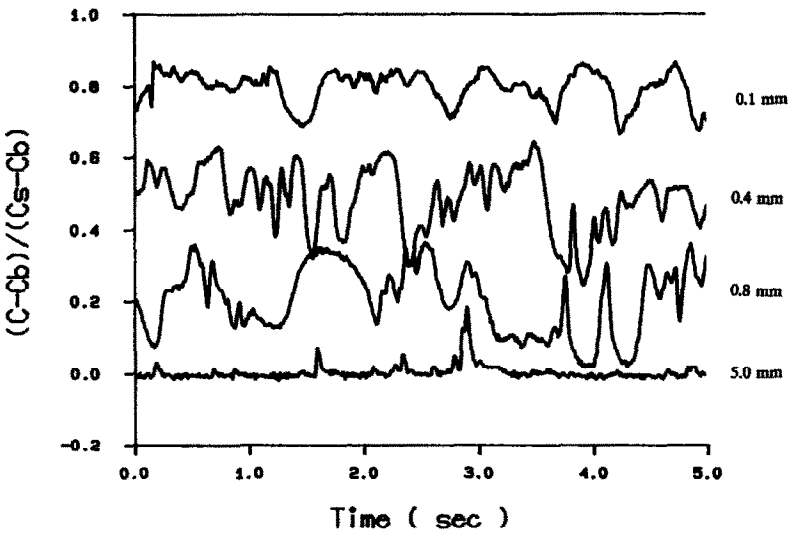

FIG. 6. Time series data of instantaneous concentration for grid condition #3 at 0.1, 0.4, 0.8 and 5.0 mm submergence. (Note these measurements are not simultaneous.)

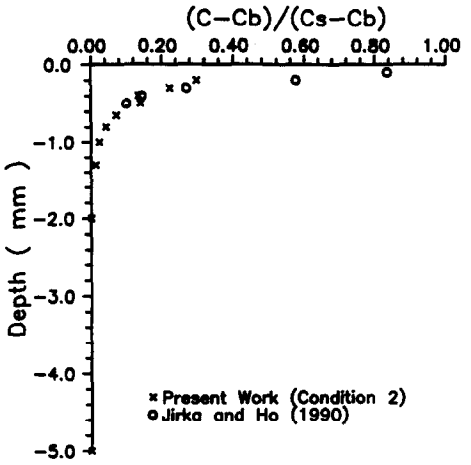

FIG. 7. Mean concentration profiles of grid condition #2.

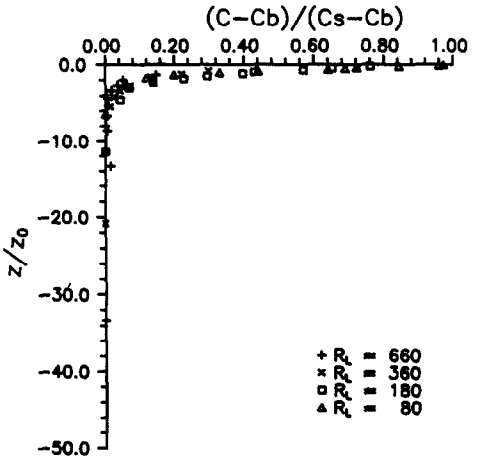

FIG. 9(a). Mean concentration profiles with normalized depth.

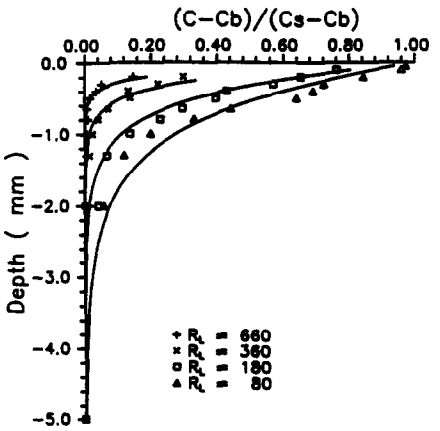

FIG. 8. Mean concentration profiles of four grid conditions, —: exponential approximations.

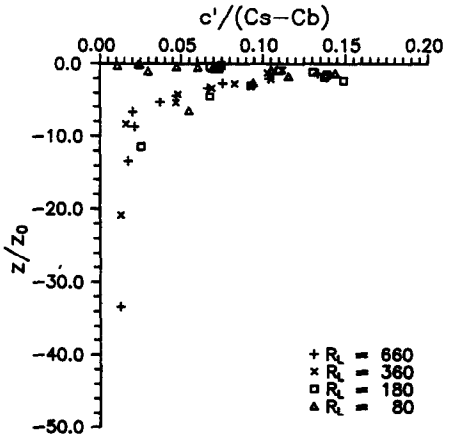

FIG. 9(b). R.m.s. concentration profiles with normalized depth.

thickness δ, and the predicted diffusive sublayer thickness L_D is given in Fig. 10(a). Except for grid condition #1, the values of z_0 and δ are remarkably close in trend and magnitude. Our data appear to be the first consistent observations that support the conceptual framework of interfacial gas transfer which is controlled by molecular diffusion in a layer whose thickness is determined, however, by turbulent activity. This consistency is emphasized again in Fig. 10(b) which shows the Lewis–Whitman film thickness δ, and the diffusive sublayer thickness L_D plotted against z_0. It shows both δ and L_D have a nominally linear relation with z_0. Since L_D is an order of magnitude estimate, this suggests a quantitative relationship

$$z_0 = \alpha L_\infty R_L^{-1/2} Sc^{-1/2} \tag{8}$$

where $\alpha \approx 0.12$ is just a scaling constant. This means that the thickness of gas boundary layer z_0 can be directly predicted from the turbulence properties and the given molecular diffusivity. Since L_D is controlled by large eddies (Brumley and Jirka [3]), this evidence points to the fact that the interfacial transfer process is dominated by large eddies, at least within the present Reynolds number range.

Finally, Fig. 11 shows the normalized transfer coefficient K_L vs the turbulent Reynolds number R_L on a log–log scale. The transfer coefficient K_L is normalized by the Hopfinger–Toly velocity U_{HT}. It also shows the best-fit curve of the data $(K_L/U_{HT}) \propto R_L^{-0.44}$ (the solid line), together with the trend of Fortescue and Pearson's [18] large eddy model $(K_L/u') \propto R_L^{-0.5}$ (dashed line). The large eddy model prediction can be written in the form

$$K_L/u = \beta R_L^{-0.5} Sc^{-0.5} \tag{9}$$

in which u is the turbulent integral velocity (see equation (3)), and β is a coefficient. Fortescue and Pearson [18] suggested a value of $\beta = 1.46$, while Theofanous *et al.* [19] proposed $\beta = 0.73$ on the basis of Brown's open-channel flow data [20]. The present data are approximated by a lower value $\beta = 0.25$ (dashed line in Fig. 11) if the present definitions of turbulent velocity (U_{HT}) and length scales (L_∞) are used. It appears that the discrepancy in the coefficient value could be

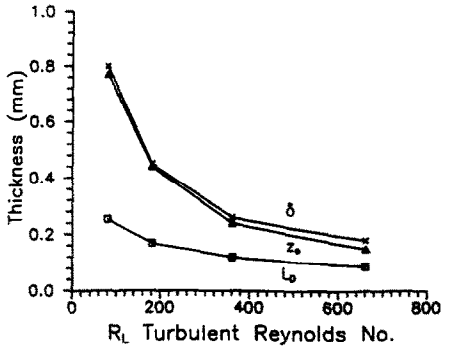

FIG. 10(a). Comparison of various scales of concentration boundary layer.

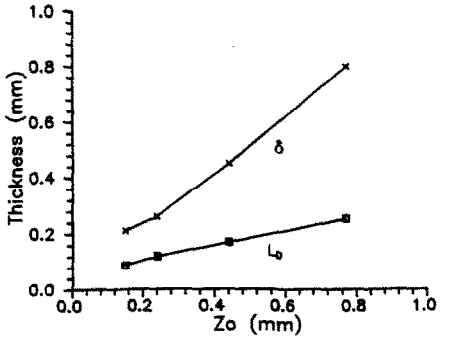

FIG. 10(b). Lewis–Whitman film thickness δ, and diffusive sublayer L_D vs the measured thickness z_0.

caused by differences in the turbulent scales definitions between stirred-grid and open-channel flow experiments. This should be the topic of a future study.

Velocity fluctuations

The profile of vertical velocity fluctuations for grid condition #2 is shown in Fig. 12. The r.m.s. vertical velocity w' and depth z has been normalized by the Hopfinger–Toly velocity U_{HT} and the integral length scale L_∞ (thickness of the surface influenced layer), respectively. The dashed curve represents the numerical fit to the source layer theory of Hunt and Graham

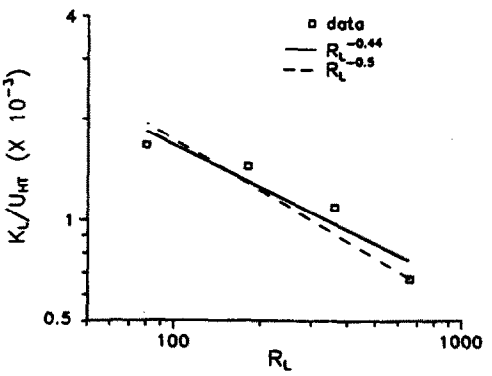

FIG. 11. Normalized transfer velocity vs turbulent Reynolds number.

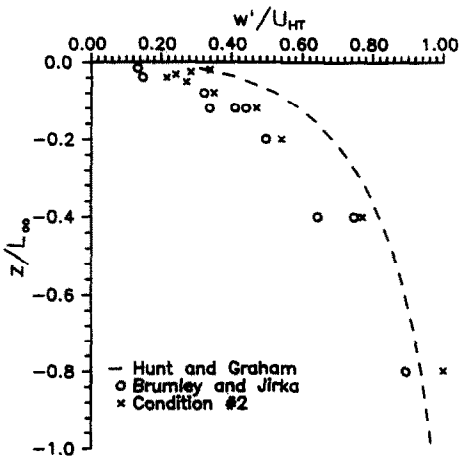

FIG. 12. Vertical velocity fluctuation profiles of grid condition #2.

[12]. Also shown in Fig. 12 are the earlier measurements of Brumley and Jirka [11]. The agreement again confirms that the source layer theory is appropriate to describe the flow field inside this surface-influenced layer.

Integral length scales of velocity and concentration

The integral length scales of the vertical velocity $4L_w$ and of the concentration L_c for the grid condition #2 from simultaneous measurements are shown in Fig. 13. Both the depth z and the integral length scales have been normalized by the longitudinal integral length scale L_∞. The integral length scales were obtained by evaluating the auto-correlation function of the desired quantity and integrating up to its first zero, then using the Taylor 'frozen turbulence' hypothesis to convert time scale to length scale. The value $4L_w$ is plotted for better comparison, since the transverse integral length scale is theoretically one

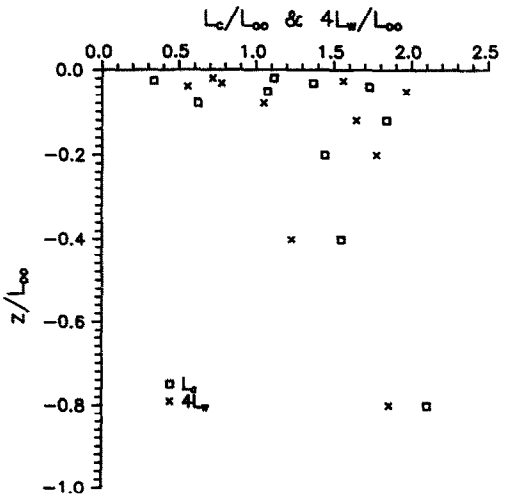

FIG. 13. Profiles of transverse and concentration integral length scales of grid condition #2.

quarter of the length scale of isotropic turbulence (Tennekes and Lumley [15]). Although there is considerable scatter in the near-surface region, this figure shows that the integral length scale for concentration fluctuation is about the same order of magnitude as the integral length scale ($2L_\infty$) for turbulent velocity. Thus, the major concentration fluctuation observed by a probe moving in the horizontal plane appears to correlate to the up- and down-welling transport associated with the large eddies. This interpretation is consistent with the earlier data (Fig. 10) which show that the observed boundary layer indeed scales with the properties of those eddies, i.e. the thickness of diffusive sublayer L_D.

Direct flux measurements

The simultaneous measurements of turbulent velocity and oxygen concentration are restricted within the concentration boundary layer due to the size of the velocity probe used in this study. Nevertheless, the vertical profiles of turbulent flux measured by the eddy correlation method are shown in Fig. 14. These measured fluxes $-\langle wc\rangle$ have been normalized by the absolute value of the mean flux J as measured in bulk transfer measurements. The dashed line is the predicted turbulent flux profile subtracting the molecular flux due to the exponential mean concentration distribution, i.e. equation (7), in the near-surface region.

In the near-surface region, the measured downward fluxes appear to be larger than the expected values. It is believed that this is due to the inaccuracies of vertical velocity measurements by a relatively large split-film probe (proximity effect) and the surface waviness giving rise to an error in the measured scalar fluxes. In the lower region, the measured downward fluxes tend to be below the mean flux. As to the reason for this discrepancy, it is speculated that the eddy correlation method is not precise enough to measure the turbulent fluxes involving large velocities but with small concentration fluctuations.

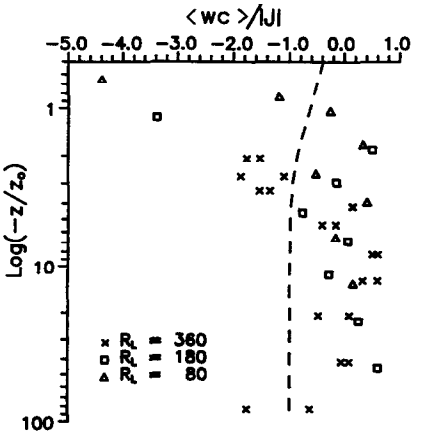

FIG. 14. Profiles of measured turbulent fluxes.

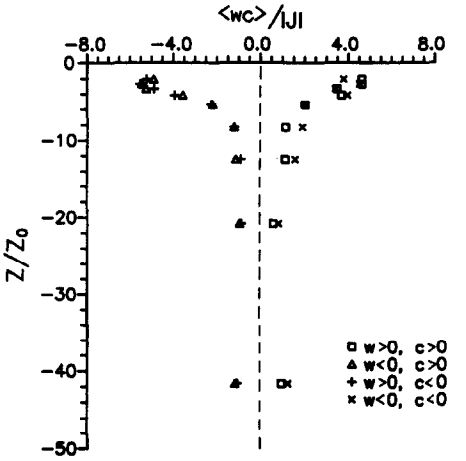

FIG. 15. Profiles of categorized flux events of grid condition #2.

This difficulty is further illustrated by Fig. 15 which shows the vertical profiles of different flux events of grid condition #2. These fluxes were calculated by classifying the instantaneous products wc into four different quadrants ($w > 0$, $c > 0$; $w > 0$, $c < 0$; $w < 0$, $c > 0$; and $w < 0$, $c < 0$), summing them separately, and then dividing by the total sample number. These fluxes have also been normalized by the absolute value of the mean flux J. This figure shows the contribution from the two different negative fluxes ($w > 0$, $c > 0$, and $w < 0$, $c < 0$) is about the same. A similar situation holds for the positive fluxes ($w > 0$, $c > 0$, and $w < 0$, $c > 0$). Thus, the up- and downward gas transport activity seems to be very energetic while the net transfer is small. Despite these difficulties and shortcomings, the direct flux measurements are within one order of magnitude of the mean flux. The value of these measurements lies more in providing qualitative insight rather than quantitative occurrences. This is further explored in the following.

Spectra

Selected vertical velocity and concentration spectral density functions are shown in Figs. 16 and 17, respectively. These spectra represent the data of grid condition #2 at submergence 0.8, 2.0 and 10 mm (or $z/z_0 = -3.33$, -8.33 and -41.7). The one-dimensional wave number κ_1 has been normalized by the constant $L_\infty^{-1} = 40\ \mathrm{m}^{-1}$. The vertical velocity spectra E_w are normalized by the constant $2U_{HT}^2 L_\infty = 2.64\ \mathrm{m \cdot mm^2 s^{-2}}$. The concentration spectra E_c are normalized by the constant $2(C_s - C_b)^2 L_\infty = 1.01\ \mathrm{m \cdot mg^2\ l^{-2}}$. The normalized wave number corresponds to the integral length scale, indicated by 'I', is equal to $\kappa_1 L_\infty = 1.8$ (Tennekes and Lumley [15]). The normalized Kolmogorov wave number, as indicated by 'K', is equal to $0.55(2\pi/\eta)/L_\infty^{-1} = 144$.

These spectra show that the turbulent energy increases with submergence, whereas the concentration fluctuation activity decreases with sub-

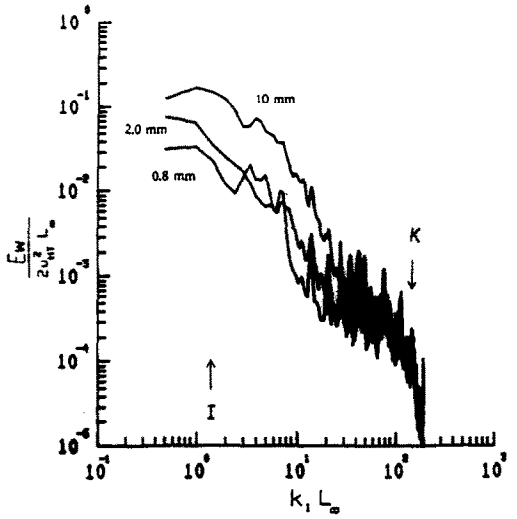

FIG. 16. Vertical velocity spectra of grid condition #2.

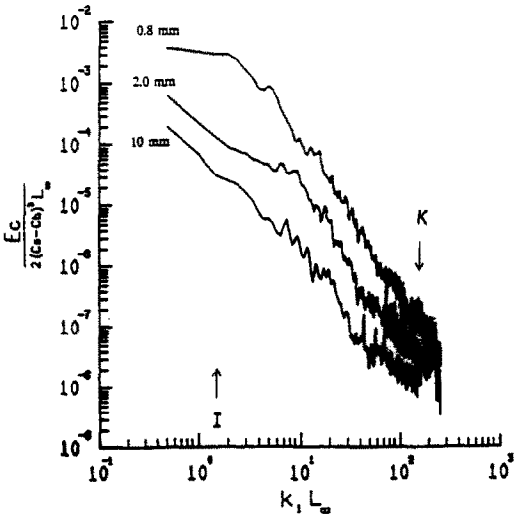

FIG. 17. Concentration spectra of grid condition #2.

mergence. The peaks in the spectrum of vertical velocity at 0.8 mm depth correspond to the surface waves associated with the grid frequency. This phenomenon does not appear in the concentration spectra indicating that surface wave problems have less effect on the interfacial concentration measurement.

It is illustrative to consider the interaction between velocity and concentration fluctuation through the cross-spectral density function which can reveal the correlation of these two different quantities at a certain wave number. The definition of the cross-spectrum E_{wc} of vertical velocity w and concentration c is the Fourier transformation of its cross-correlation function R_{wc}

$$E_{wc}(\kappa_1) = 2\int_{-\infty}^{\infty} R_{wc}(\tau)\, e^{-i2\pi\kappa_1\tau}\, d\tau$$

$$= C_{wc}(\kappa_1) - iQ_{wc}(\kappa_1) \tag{10}$$

where the real part, C_{wc}, is called the coincident spectral (or co-spectral) density function, the imaginary part, Q_{wc}, the quadrature spectral (or quad-spectral) density function (Bendat and Piersol [21]). The cross-spectral density function is defined as one-sided, i.e. $0 < \kappa_1 < \infty$. Therefore, the average product of w and c can be related to the co-spectrum C_{wc} in the following way

$$\langle wc \rangle = R_{wc}(0)$$

$$= \int_0^{\infty} C_{wc}(\kappa_1)\, d\kappa_1. \tag{11}$$

This equation implies that the co-spectrum C_{wc} contains the information on how much the co-variance contributes at a certain wave number interval.

The normalized co-spectral density function C_{wc} for grid condition #2 is shown in Fig. 18. The spectra have been normalized by the constant $2U_{HT}(C_s - C_b)L_\infty = 1.636$ mg m^{-1} s^{-1}. Although these co-spectra are limited as discussed above, the contribution to the total flux from the product of w and c associated with the small wave number region seems considerably bigger than that for the high wave number region. This appears to be yet another indication that the large scale eddy motions are controlling the interfacial mass transfer process.

CONCLUSIONS

The present study reports the first concurrent measurements of near-surface turbulent velocity and

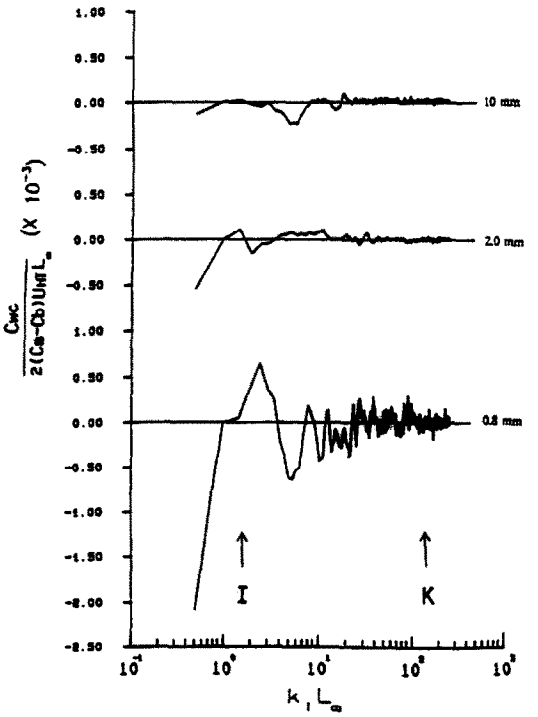

FIG. 18. Co-spectra of vertical velocity and concentration of grid condition #2.

concentration fluctuations, together with bulk transfer measurements under well-controlled turbulence conditions, which are representative environmental situations. In the Reynolds number range of the experiments (R_L = 80–660), the results show strong and consistent evidence for the large eddy control of the interfacial transfer process. This is demonstrated by several interrelated facts.

(1) The thickness of observed gas boundary layer z_0 scales with the diffusive sublayer L_D, which is controlled by large eddies.

(2) The best-fit curve for the bulk transfer velocity shows a Reynolds number dependence consistent with a large eddy model prediction.

(3) The integral length scale for concentration fluctuations is of about the same order of magnitude as the integral length scale for turbulent vertical velocity fluctuations.

(4) The co-spectra of velocity and concentration fluctuations indicate that most of the contribution to the total flux occurs in the small wave number region, i.e. large eddy motions.

As a next step in covering a wider class of hydrodynamic conditions, it seems obvious and imperative to attempt similar direct measurements at much higher Reynolds number conditions. This will allow validation of the conjecture of Theofanous *et al.* [19] for a dual regime behavior with small eddy domination at higher R_L. Clearly, such measurements will present substantial technical difficulties due to the yet smaller boundary layer thickness in that range. Nevertheless, they should be attempted perhaps using different facilities and/or measurement techniques.

Acknowledgements—This study was supported by the United States Geological Survey through grant No. 14-08-0001-G1480. Additional support in the data analysis phase was provided by NOAA Sea Grant No. 431-S213N.

REFERENCES

1. M. Coantic, Mass transfer across the ocean–air interface: small scale hydrodynamic and aerodynamic mechanisms, *PhysicoChem. Hydrodyn.* **1**, 249–279 (1980).
2. T. G. Theofanous, Conceptual models of gas exchange. In *Gas Transfer at Air–Water Interfaces* (Edited by W. Brutsaert and G. H. Jirka), pp. 271–281 (1984).
3. H. B. Brumley and G. H. Jirka, Air–water transfer of slightly soluble gases: turbulence, interfacial processes and conceptual models, *PhysicoChem. Hydrodyn.* **10**(3), 295–319 (1988).
4. S. Luk and Y. Lee, Mass transfer in eddies close to air–water interface, *A.I.Ch.E.* **32**(9), 1546–1554 (1986).
5. W. E. Asher and J. F. Pankow, The interaction of mechanically generated turbulence and interfacial films with a liquid phase controlled gas/liquid transport process, *Tellus* **38B**, 305–318 (1986).
6. G. H. Jirka and A. W.-K. Ho, Gas transfer at the water surface: measurements of gas concentration fluctuations, *J. Hydraul. Engng, ASCE* **116**(6), 835–846 (1990).
7. B. Jähne, From the measurement of mean fluxes to a detailed experimental investigation of the gas transfer process at a free wavy water surface, *Proc. 2nd Int. Symp. on Gas Transfer at Water Surfaces* (1991).
8. L. M. Wolff, Z. C. Liu and T. J. Hanratty, Use of fluorescence techniques to study the time-varying concentration close to an interface, *Proc. 2nd Int. Symp. on Gas Transfer at Water Surfaces* (1991).
9. W. K. Lewis and W. G. Whitman, Principles of gas absorption, *Ind. Engng Chem.* **16**, 1215–1220 (1924).
10. E. J. Hopfinger and J. A. Toly, Spatially decaying turbulence and its relation to mixing across density interfaces, *J. Fluid Mech.* **78**, 155–175 (1976).
11. H. B. Brumley and G. H. Jirka, Near-surface turbulence in a grid-stirred tank, *J. Fluid Mech.* **183**, 235–263 (1987).
12. J. C. R. Hunt and J. M. R. Graham, Free-stream turbulence near plane boundaries, *J. Fluid Mech.* **84**, 209–235 (1978).
13. Y. Lee, G. T. Taso and P. C. Wankat, Ultramicroprobe method for investigating mass transfer through gas–liquid interfaces, *Ind. Engng Chem. Fundam.* **17**(1), 59–66 (1978).
14. C. R. Chu, Near-surface turbulent velocity and oxygen concentration measurements in a grid-stirred tank, M.S. Thesis, Cornell University (1990).
15. H. Tennekes and J. L. Lumley, *A First Course in Turbulence*. MIT Press, Cambridge, MA (1972).
16. A. W.-K. Ho, A study of oxygen transfer at the air–water interface of a grid-agitated tank, M.S. Thesis, Cornell University (1987).
17. J. C. R. Hunt, Turbulence structure and turbulent diffusion gas–liquid interface. In *Gas Transfer at Air–Water Interfaces* (Edited by W. Brutsaert and G. H. Jirka), pp. 67–80 (1984).
18. G. E. Fortescue and J. R. Pearson, On gas absorption into a turbulent liquid, *Chem. Engng Sci.* **22**, 1163–1176 (1967).
19. T. G. Theofanous, R. N. Houze and L. K. Brumfield, Turbulent mass transfer at free, gas–liquid interface, with applications to open-channel, bubble and jet flows, *Int. J. Heat Mass Transfer* **19**, 613–624 (1976).
20. L. C. Brown, Oxygen transfer in open channel flow, Ph.D. Thesis, University of Wisconsin (1970).
21. J. S. Bendat and A. G. Piersol, *Random Data: Analysis and Measurement Procedures*. Wiley–Interscience, New York (1986).

MESURE DU FLUX GAZEUX TURBULENT SOUS L'INTERFACE AIR–EAU D'UN RESERVOIR AGITE PAR UNE GRILLE

Résumé—On conduit des expériences pour comprendre le mécanisme du transfert interfacial de gaz gouverné par le côté liquide. La turbulence du liquide près de la surface et les fluctuations de concentration en oxygène sont mesurées dans un réservoir agité par une grille pour un domaine de nombre de Reynolds R_L entre 80 et 660. On observe que l'épaisseur de la couche limite s'accorde avec celle du film de Whitman déterminée à partir du changement de concentration globale. La dépendance fonctionnelle au nombre de Reynolds turbulent est cohérente avec une grande domination turbulente. Des mesures simultanées additionnelles des fluctuations turbulentes de vitesse et de concentration d'oxygène, incluant des mesures directes de flux, montrent que les mouvements turbulents à grande échelle sont plus efficaces dans le mécanisme de transfert interfacial de masse.

MESSUNG DER TURBULENTEN GASSTROMDICHTE UNTERHALB DER LUFT/WASSERGRENZFLÄCHE IN EINEM BEHÄLTER, IN DEM MIT EINEM GITTER GERÜHRT WIRD

Zusammenfassung—Es werden Experimente durchgeführt, mit dem Bestreben, die Einzelheiten der Mechanismen für den Gastransport durch die Grenzfläche zur Flüssigkeit aufzuklären. Oberflächennahe Turbulenzen in der Flüssigkeit und Fluktuationen der Sauerstoffkonzentration wurden in einem Labor-Rührbehälter für einen Bereich der turbulenten Reynolds-Zahl R_L von 80–660 gemessen. Unsere Beobachtungen zeigen, daß die Dicke der Gasgrenzschicht in Richtung und Größe streng mit der Lewis/Whitman-Filmdicke übereinstimmt, die aus der Konzentrationsänderung der Gesamtmasse berechnet wurde. Weiterhin stimmt die funktionale Abhängigkeit von der turbulenten Reynolds-Zahl mit dem Vorherrschen großer Wirbel überein. Zusätzlich geben gleichzeitige Messungen der turbulenten Geschwindigkeit und der Fluktuationen der Sauerstoffkonzentration (einschließlich direkter Strömungsmessungen) weitere Hinweise darauf, daß großräumige Wirbelbewegungen den Stofftransport durch die Grenzfläche stärker beeinflussen.

ИЗМЕРЕНИЯ ТУРБУЛЕНТНОГО ПОТОКА ГАЗА ПОД ГРАНИЦЕЙ РАЗДЕЛА ВОЗДУХ–ВОДА В ЕМКОСТИ С ПЕРЕМЕШИВАЮЩИМИ РЕШЕТКАМИ

Аннотация—Экспериментально исследуется механизм переноса газа на границе раздела со стороны жидкости. Турбулентность жидкости и колебания концентрации кислорода у поверхности измерялись в лабораторной емкости с перемешивающими решетками при турбулентном числе Рейнольдса R_L, изменяющемся в диапазоне 80–660. Наблюдения показывают, что толщина пограничного слоя газа совпадает по тенденции изменениях величине с толщиной пленки Льюиса–Уитмэна, определяемой по изменения объемной концентрации. Наличие функциональной зависимости от турбулентного числа Рейнольдса указывает на преобладание вихрей. Дополнительные одновременные измерения флуктуаций турбулентной скорости и концентрации кислорода, включающие прямые измерения потока, также свидетельствуют о том, что крупномасштабные вихревые движения более эффективны в процессе массопереноса на границе раздела.